Catal Lett (2017) 147:1051–1060
DOI 10.1007/s10562-017-1995-7

Ionic Liquid Mediated In Situ Synthesis of Ru Nanoparticles for CO_2 Hydrogenation Reaction

Praveenkumar Ramprakash Upadhyay[1] · Vivek Srivastava[1]

Received: 4 October 2016 / Accepted: 8 February 2017 / Published online: 20 February 2017

Abstract We straightforwardly synthesized nine different types of ruthenium nanoparticles by using a series of ruthenium metal precursors and ionic liquids. All the materials went for XRD, XPS and SAXS analysis, before going to CO_2 hydrogenation reaction as catalyst. As per the results, it was clear that the coordination between anions of ionic liquids and ruthenium nanoparticles played an important role with respect to their catalytic performance in CO_2 hydrogenation reaction. Surprisingly, less coordinated and large [DAMI][TfO] mediated ruthenium nanoparticles gave better results over other developed catalytic systems. Narrow size well distributed and stable insitu generated ruthenium nanoparticles were synthesized and found highly active in terms of formic acid formed during the CO_2 hydrogenation reaction to other ionic liquid immobilized standing ruthenium nanoparticles. Low catalyst loading, ligand free approach, simple reaction protocol, easy product isolation steps and seven times catalyst recycling are major outcomes of this proposed work.

Graphical Abstract

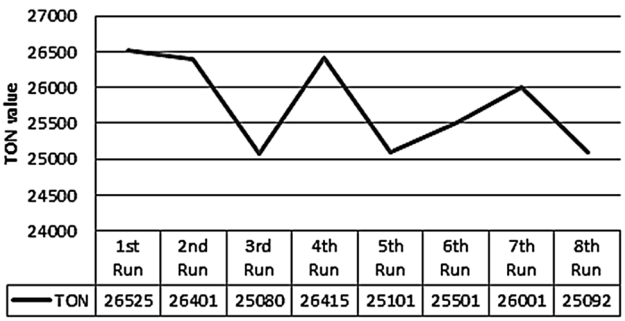

Keywords Ruthenium nanoparticles · Hydrogenation reaction · Formic acid · Carbon sequestration

1 Introduction

The growing concentrations of greenhouse gases (GHGs) in our atmosphere are highly connected to global warming [1–3]. Among GHGs, carbon dioxide is the one of the most important greenhouse gas [1, 4]. The emissions from fossil fuel combustion are the main source of CO_2 production in our atmosphere. The reduction of CO_2 emission into the atmosphere is an urgent necessity as it is highly responsible for the greenhouse effect. Various physical as well as chemical techniques have been applied to consume exhausted CO_2, such as fixation in carbonates, geological or ocean storage or afforestation, pulp and paper, food, beverage, and metal industries [4–6]. Unfortunately, these methods hurt with many disadvantages in terms of financial factors, safety, productivity, and dependability of their instant application [4, 7]. The catalytic conversion of CO_2 into the valuable chemical is considered as a significant substitute,

Electronic supplementary material The online version of this article (doi:10.1007/s10562-017-1995-7) contains supplementary material, which is available to authorized users.

✉ Vivek Srivastava
vivek.shrivastava@niituniversity.in

[1] Basic Sciences: Chemistry, NIIT University, NH-8 Jaipur/Delhi Highway, Neemrana, Rajasthan 301705, India

where we can't only to capture, but we also use CO_2 gas to synthesize added value chemicals [4, 8–10]. However, CO_2 is extensively acknowledged as a reactant for the synthesis of carbonates and other important chemicals such as methanol, aspirin, formic acid etc, but CO_2 reduction is still a key task for the scientific community due to the tremendous thermodynamic stability of CO_2 molecule. In the view of the extraordinary stability of CO_2, it's a major challenge to develop competent and extremely reductive procedure to make them ready for chemical reaction [4, 7, 10, 11].

Metal nanoparticles (with diameter 1–10 nm) carry exclusive properties mainly because of their exclusive quantum size effects and large surface-to-volume ratio [12, 13]. In order to get kinetically stable and well dispersed metal nanoparticles, stabilizer (polymers, surfactants, polyoxoanion) is required to prevent agglomeration process which eventually leads to the development of the bulk metal (which is thermodynamically favored) [12–21]. Apart from mentioned methods, inorganic supports such as clay, TiO_2, zeolite, silica, etc. were also exploited for the same task. Properties of supported metal nanoparticles is mainly depends on the characteristics (size, shape, composition) of metal nanoparticles and theirs dispersion over support [20–24]. Hence, metal support interaction deeply affects the electronic properties of metal. In addition, the metal–support interface also impact sometimes on the nanoparticle morphology in a very unusual way, hence also affect their catalytic properties in a negative manner [24].

Many transition metals were tested as an active and promising nanocatalyst for the selective hydrogenation of CO_2 gas. In several reports Ru, Pd, Pt, Rh, and Zn nanometals were supported on organic–inorganic supports (polymeric, ionic liquids, silica, clay, zeolite, etc.) to positively alter the CO_2 hydrogenation reactions, but regrettably, in most of the reports, above mentioned catalytic systems undergo with the dull catalyst synthesis practice, high catalyst loading and catalyst leaching during recycling experiments [11–20].

Ionic liquids (ILs) are organic salt have immeasurably low or negligible vapor pressure, good thermal stability, wide temperature range and strong solvating power for various substances (good solubility of heterogeneous/homogeneous catalytic systems) [25–28]. Therefore, ionic liquids were considered as a good alternative for toxic conventional solvent systems. We and others have recently published various reports on imidazolium based ionic liquids as a stabilizer for the synthesis of catalytically active transition metal nanoparticles [25–31]. Imidazolium ionic liquids possess pre-organized structures, mainly through hydrogen bonds that induce structural directionality, as opposed to classical salts in which the aggregates display charge-ordering structures [31–39]. These ILs structures can adapt or are adaptable to many species, as they provide hydrophobic or hydrophilic regions and a high directional polarizability. This structural organization of ILs can be used as "entropic drivers" for natural, well-defined, and prolonged ordering of nanoscale assemblies [40–42]. Indeed, we have used imidazolium ionic liquids as a template, stabilizer, and solvent for the synthesis of a plethora of transition-metal nanoparticles [42, 43]. Ionic liquid mediated well dispersed transition-metal nanoparticles are reported as stable and highly active catalysts for various reactions, even under harsh reaction condition (high temperature and pressure). The promising catalytic properties (like activity and selectivity) of these ionic liquid immobilized metal nanoparticles mainly appear as they possess a pronounced surface like (multi-site) rather than single-site-like catalytic properties [40–47]. In other cases, the metal nanoparticles are not stable and tend to aggregate/agglomerate or serve as simple reservoirs for mononuclear catalytically active species [10–13].

ILs were also utilized in the extraction and absorption of CO_2, SO_2, H_2S and N_2 gases [32–37] (by varying cations or anions or by grafting functional groups onto the ions). The above mentioned unique properties and applications of ionic liquid were also exploited in our report by performing a separate absorption study under different time, temperature and other reaction conditions in order to get best CO_2 absorption result with ionic liquid (which directly affect the selectivity of reaction.) We synthesized a series of ionic liquids and tested them as reaction medium to prepare insitu Ru nanoparticles and to capture partial CO_2 hydrogenated products (formic acid). Additionally, use of ionic liquid also offers easy catalyst isolation and catalyst recycling steps during the CO_2 hydrogenation reaction.

2 Experimental

All the chemicals were purchased from Sigma Aldrich, Acros or Fluka. Nuclear Magnetic Resonance (NMR) spectra were recorded on standard Bruker 300WB spectrometer with an Avance console at 400 and 100 MHz for ^1H and ^{13}C NMR respectively. All the reaction was carried out in 100 mL Fisher Porter Bottle, Sigma Aldrich. The catalyst material was characterized by TEM (Hitachi S-3700N). High-resolution mass spectra (HRMS) were measured on a VG Auto-spec-Micromass spectrometer (EI) or in a Waters Q-Tof Ultima API (ESI).

2.1 CO_2 Loading on Ionic Liquids [30]

In a typical procedure, the CO_2 capture was carried out in high pressure autoclave (100 mL). The absorbents were charged into the reactor at room temperature. Then, the air in the flask was replaced by passing CO_2. The absorption

was conducted at 80 °C with a 4 bar CO_2 gas for 1 h. The amount of CO_2 absorbed was determined by calculating the weight of the reaction mixture with an analytical balance. Data points were taken with an accuracy of ±0.0001 g every 5 min. At 80 °C slight while at 100 °C complete desorption of CO_2 was recorded.

2.2 Sample Preparation Procedure for TEM Analysis

In TEM analysis, a drop of the suspension containing the Ru nanoparticles embedded in the IL was allowed to disperse in isopropanol. A very small quantity of this dispersion was placed on a carbon-coated copper grid. Digital images were used to determine particle size of Ru nanoparticles. Nanoparticle diameters were estimated from groups of 200 particles (400 counts) chosen in random areas of the enlarged micrographs. The diameters of the particles in the micrographs were measured using Sigma Scan Pro 5.

2.3 Synthesis of Standing Ru NPs in Ionic Liquid

The high pressure autoclave was charged with precursor (0.5 g) and ionic liquid (1 g) as per Table 1. The reaction was allowed to stir under argon atmosphere (2 bar) for 1 h at room temperature. Later, argon was replaced by hydrogen gas and reaction mass was stirred under hydrogen atmosphere (4 bar) for 2 h at 50 °C. After cooling the reaction mass, gaseous pressure of reaction vessel was released and Ru NPs with ionic liquid was washed with diethyl ether (5 × 2 mL). Further, Ru NPs with ionic liquid was dried under high vacuum to remove all the volatile impurities.

2.4 Reaction Protocol for Ionic Liquid Mediated Ru NPs for CO_2 Hydrogenation Reaction

The Fischer Potter bottle was charged with 0.25 g of ionic liquid mediated Ru NPs and water (2 mL). Then the oxygen of reaction vessel was replaced by CO_2/H_2 gas. Reaction mass was allowed to stir for 5 h at 100 °C. Later the reaction vessel was allowed to cool (2–5 °C) with the help of cold water. A small amount of crude reaction mass was used for ^{1}HNMR analysis. Water was evaporated from the reaction mass at 110 °C, than formic acid was isolated from the reaction mass with the help of nitrogen gas flow at 125–130 °C, passing through the water trap, in order to capture formic acid. Acid base titration was used to calculate the amount formic acid in water trap. The results obtained from ^{1}HNMR analysis as well as from titration method were full agreement.

2.5 In situ Generation of Ru NPs in Ionic Liquid for the CO_2 Hydrogenation Reaction and Recycling Experiment

The Fischer Potter bottle was charged with ruthenium precursor $[RuCl_2(C_6H_6)]_2$ (0.100 g) and ionic liquid [DAMI][TfO](0.210 g). After stirring the reaction mass under argon (1 bar) for 1 h at room temperature, the argon gas was replaced with hydrogen gas (2 bar) and then the reaction was allowed to stir for next 2 h at 50 °C. Later, the reaction mass was allowed to cool and the pressure was released. After flushing the reaction mass with 2–3 times with argon gas, water was added to the reaction mass using addition funnel of Fisher Potter's bottle. Then, the reaction vessel was charged with CO_2 and H_2 gas (desired quantity) by

Table 1 Absorption study of CO_2 over ionic liquids

Ionic liquid	CO_2 pressure (bar)	Temperature (°C)	Time (h)	CO_2 Loading[a]
[mammim][NTf_2]	20	50	1	26
[mammim][TfO]	20	50	1	42
[mammim] [$CF_3CF_2CF_2CF_2SO_3$]	20	50	1	48
[mammim] [BF_4]	20	50	1	14
[DAMI][TfO]	20	50	1	53
[DAMI][NTf_2]	20	50	1	50
[DAMI][$CF_3CF_2CF_2CF_2SO_3$]	20	50	1	69
[DAMI][BF_4]	20	50	1	22
[DAMI][$CF_3CF_2CF_2CF_2SO_3$]	10	50	1	32
[DAMI][$CF_3CF_2CF_2CF_2SO_3$]	25	50	1	71
[DAMI][$CF_3CF_2CF_2CF_2SO_3$]	20	80	1	66
[DAMI][$CF_3CF_2CF_2CF_2SO_3$]	20	100	1	36
[DAMI][$CF_3CF_2CF_2CF_2SO_3$]	20	50	3	70
[DAMI][$CF_3CF_2CF_2CF_2SO_3$]	20	50	0.5	24

[a]Mole of CO_2 captured per mole of ionic liquid

replacing the argon atmosphere and the total reaction mass was allowed to stir for next 5 h at 100 °C. After cooling the reaction mass using ice cold water (2–5 °C), gas pressure was released. A small amount of crude reaction mass was used for ^{1}HNMR analysis. Water was evaporated from the reaction mass at 50 °C, then formic acid was isolated from the reaction mass with the help of nitrogen gas flow at 75–80 °C, passing through the water trap, in order to capture formic acid. Acid base titration was used to calculate the amount formic acid in water trap. The results obtained from ^{1}HNMR analysis as well as from titration method were in full agreement. Ionic liquid mediated Ru- NPs were washed with diethyl ether (5 × 2 mL) and dried under required pressure for 12 h at 50 °C (All the product isolation steps as well as catalyst cleaning steps were carried out in the Fischer Potter bottle to avoid the catalyst loss). Then the catalytic system went for recycling experiment where, the [DAMI] [TfO] ionic liquid immobilized Ru NPs were allowed to stir under argon atmosphere (2 bars) for 1 h at room temperature. Later, argon was replaced by hydrogen gas and reaction mass was stirred under hydrogen atmosphere (4 bars) for 2 h at 50 °C and then all the steps were completed as per above mentioned CO_2 hydrogenation protocol.

3 Result and Discussion

3.1 Solubility of CO_2 Gas in Functionalized Ionic Liquids

In some of recent reports, ionic liquids were utilized to capture carbon dioxide gas [32, 33]. We synthesized and tested the absorption performance of the following functionalized ionic liquids; Ionic liquids like 1-(*N,N*-dimethylaminoethyl) 2,3-dimethylimidazolium trifluoromethanesulfonate ([mammim][TfO]), 1,3-di(N,N-dimethylaminoethyl)-2-methylimidazolium bis (trifluoromethylsulfonyl) imide ([DAMI][NTf2]), 1-(N,N-dimethylaminoethyl) 2,3-dimethylimidazolium bis (trifluoromethylsulfonyl) imide ([mammim][NTf2]), 1-(N,N-dimethylaminoethyl)- 2,3-dimethylimidazolium nonafluorobutanesulfonate ([mammim] [CF3CF2CF2CF2SO3]), 1-(N,N-dimethylaminoethyl)-2,3-dimethylimidazolium trifluoromethanesulfonate ([mammim] [BF4]), 1,3-di(N,N-dimethylaminoethyl)-2-methylimidazolium trifluoromethanesulfonate ([DAMI] [TfO]),, 1,3-di(N,N-dimethylaminoethyl)-2-methylimidazolium nonafluorobutanesulfonate ([DAMI][CF3CF2CF-2CF2SO3]) and 1,3-di(N,N-dimethylaminoethyl)-2-methylimidazolium tetrafluoroborate ([DAMI][BF4]) treated at the 50 °C for 1 h in high pressure autoclave with 20 bar CO2 gas (Table 1 supporting information). Among all the ionic liquids, we obtained the maximum solubility of CO2 in [DAMI][CF3CF2CF2CF2SO3] ionic liquid reaction medium. It was clearly observed from (Table 1) that the CO2 solubility in ionic liquids mainly depends on the presence of branched chains or polar groups and CO2-philic groups in the anionic or cationic parts of the ionic liquid structure. Such modifications in ionic liquid morphology increase the free volume to accommodate CO2 gas [31–37]. In addition, the physiochemical property of anions of ionic liquid plays a significant role in the solubility of CO_2 gas than the cations [35, 38]. Ionic liquid, carrying highly fluorinated anions were recorded to have the highest CO_2 solubility among the ionic liquids with the same cations [30]. Apart from such advantages, C-F bond of anions increases the rigidity and decreases the polarity of ionic liquid [31–34]. Such change in the properties of ionic liquid, not only leads to higher gas solubility in highly fluorinated as well as sulphonated ionic liquids, but also makes easier the regeneration of the ionic liquid.

3.2 Synthesis of Ru Metal Nanoparticles in Functionalized Ionic Liquids

After getting best CO_2 solubility results with [DAMI] [CF3CF2CF2CF2SO3] ionic liquid, we applied the same ionic liquid for the synthesis of ruthenium nanoparticle (Ru-NP) synthesis. Four different types of Ru precursors (such as [RuCl2 (C6H6)] 2, [Ru (COD) (2-methylallyl) 2], trans-RuCl2 (DMSO) 4, [Ru (COD) Cl2] and [Ru (COD) (COT)]), were reduced under hydrogen atmosphere in the [DAMI] [CF3CF2CF2CF2SO3] ionic liquid reaction medium at 50 °C as it is documented that nanoparticles with small size may easily get agglomerate at higher temperature [40, 41].

Initially, we stirred the well dispersed suspension of [Ru(COD)(2-methylallyl)$_2$] with [DAMI][$CF_3CF_2CF_2CF_2SO_3$] ionic liquid under argon for 1 h and while adding the hydrogen gas to suspension, the color turns black from off white within 15 min. While, [DAMI] [TfO] ionic liquid took, 35 min to get a black color suspension. After, 5 h of stirring, volatile impurities like cyclooctane, isobutene etc. were removed under high vacuum to obtain ionic liquid mediated Ru NPs.

X-ray diffraction (XRD) patterns were recovered to study the phase, purity and crystallite size of the Ru nanoparticles by using XRD Philips X'PERT MRD X-ray diffractometer equipped with a curved graphite crystal (Fig. 1). The typical diffraction pattern shows that the Ru-NPs prepared from four different Ru metal precursors in different ionic liquids confirmed their crystalline nature and high purity. The crystallite size of the Ru-NPs was calculated from the most intense diffraction peak (101) using the Debye–Scherrer's equation. All the results were summarized in Table 2. The relative intensity of the diffraction peaks of Ru-NPs

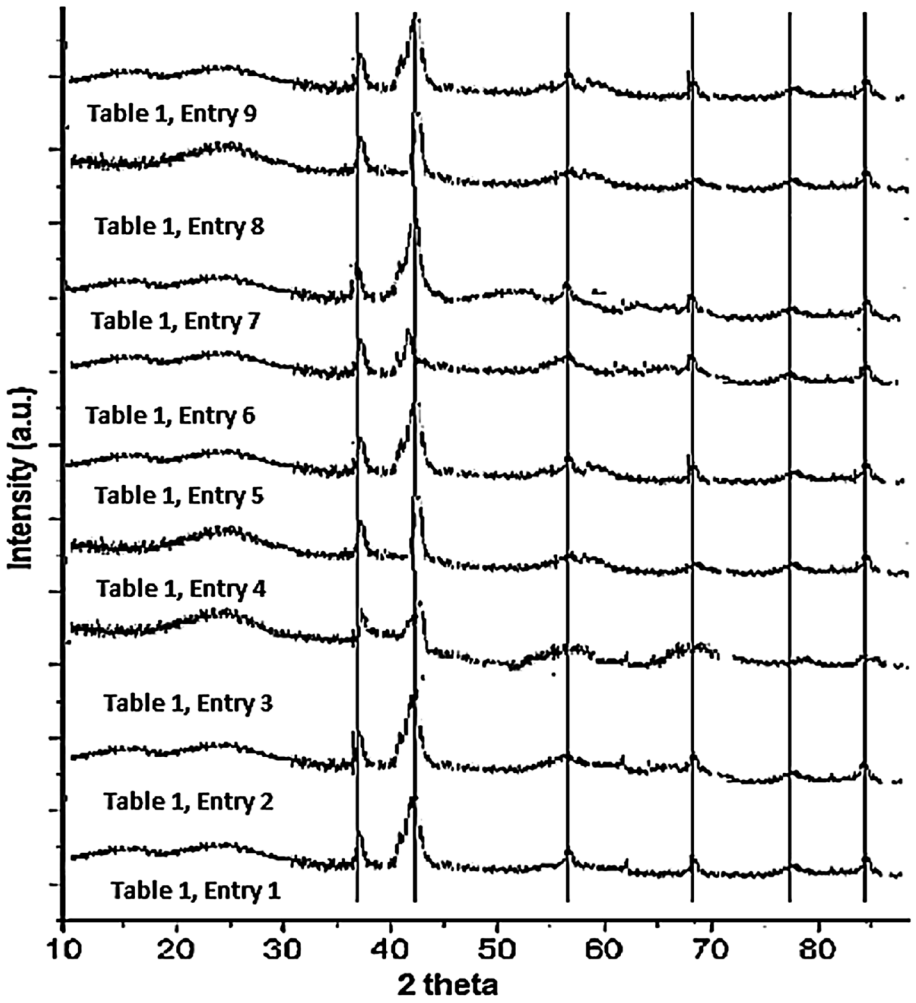

Fig. 1 XRD analysis results of Ru NPs

Table 2 Types of synthesized Ru metal catalyst

Entry	Ru metal precursors	Ionic liquid	Size of Ru NPs (±0.5 nm)[a]	Size of Ru NPs (nm)[b]	Size of Ru NPs (nm)[c]	ICP-AES values (wt% Ru)
1	$[RuCl_2(C_6H_6)]_2$	$[DAMI][CF_3CF_2CF_2CF_2SO_3]$	7.1	7.6	7.8	1.15
2	$[Ru(COD)(2\text{-methylallyl})_2]$	$[DAMI][CF_3CF_2CF_2CF_2SO_3]$	7.9	8.5	8.3	1.13
3	*trans*-$RuCl_2$ $(DMSO)_4$	$[DAMI][CF_3CF_2CF_2CF_2SO_3]$	12.1	13.2	13.4	1.13
4	$[Ru\ (COD)Cl_2]$	$[DAMI][CF_3CF_2CF_2CF_2SO_3]$	9.2	10.4	10.1	1.09
5	[Ru (COD)(COT)]	$[DAMI][CF_3CF_2CF_2CF_2SO_3]$	9.5	11.6	10.5	1.10
6	$[RuCl_2(C_6H_6)]_2$	[DAMI][TfO]	8.5	9.6	9.7	1.14
7	$[Ru(COD)(2\text{-methylallyl})_2]$	[DAMI][TfO]	8.1	9.3	8.9	1.11
8	$[RuCl_2(C_6H_6)]_2$	[mammim] $[CF_3CF_2CF_2CF_2SO_3]$	13.8	14.1	13.9	1.01
9	$[RuCl_2(C_6H_6)]_2$	[mammim][TfO]	14.1	14.9	14.8	0.98

[a]Determined by TEM analysis

[b]Calculated from XRD analysis

[c]Calculated from SAXS analysis

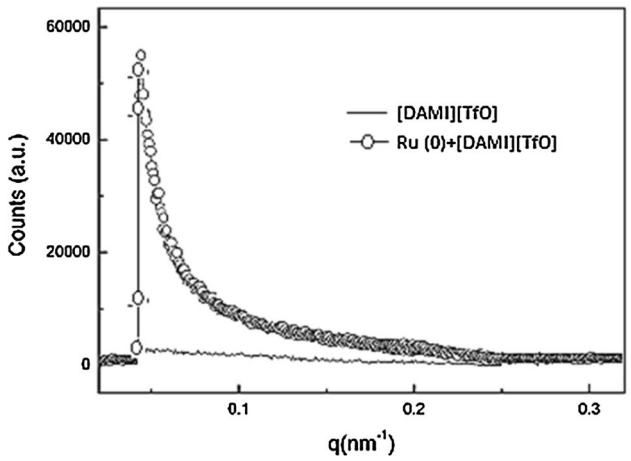

Fig. 2 SAXS spectra pattern of [DAMI][TfO] and Ru(0)+ [DAMI] [TfO]

Table 3 Results obtained from correlation and interface distribution functions

Sample	Correlation function *y*(r)		Interface distribution function g(*r*)	
	L (Å)	L_m (Å)	L (Å)	L_m (Å)
Ru (0) + [DAMI][$CF_3CF_2CF_2CF_2SO_3$]	158	82	152	88
[DAMI][$CF_3CF_2CF_2CF_2SO_3$]	112	57	120	63
Ru (0) + [DAMI][TfO]	167	76	172	83
[DAMI][TfO]	125	49	121	51

(prepared with different ionic liquids) deviated from one to one, suggesting that an each ionic liquid has different nanostructures in certain directions of the growing material. A broad peak at 42.2° clearly corresponds to metallic Ru (0), this indicates the formation of Ru nanoparticles with a size of ranges from 17.1 to 22.6 nm for different samples Table 2, entry 1–9. In contrast, additional sharp peaks centered at 38.5°, 44.2°, 58.5°, 69.5°, 78.7°, and 85.3° respectively were attributed to the presence of metallic Ru species (PDXL ver. 2.3.1) [48, 49].

The X-ray photoelectron spectroscopy (XPS, ESCALAB 250 analyzer) spectrum (Fig. 1, supplementary information) showed typical Ru(0) absorptions at 280.07 and 284.47 eV for $3d_{5/2}$ and $3d_{3/2}$, respectively, with a $\Delta = 4.40$ eV, which is consistent with literature results [46]. All the samples for XPS analysis were prepared in an argon atmosphere to guard against oxide formation; no evidence RuO_2 contamination was found in the XPS results [50].

Small angle X-ray scattering (SAXS) is a very important technique to disclose the size, shape and internal structure of colloidal particles in solution [51]. The typical SAXS spectra was recorded for [DAMI][TfO] and Ru(0) + [DAMI][TfO] and represented in Fig. 2. We measured the SAXS background scattering of ionic liquid (with and without Ru-NPs) with respect to the primary incident beam. Then, we corrected the scattering data obtained after subtracting the background noise. All the SAXS analysis and calculation were performed as per reported literature [51–67]. The X-ray scattering is experimentally calculated as a function of the vector, q [51–57]. The correlation function $y(r)$, is used to measure the electron density in a sample defined as the Fourier transform of the Lorentz-corrected SAXS profile [62–64]. The interface distribution function $g(r)$ is the Fourier transform of the interference function $G(q)$.The application of correlation and surface distribution function is accepted only in SAXS range data ($0.1\ nm^{-1} < q < 2.5\ nm^{-1}$) [63, 64].

The SAXS analysis helped to establish the correlation function between pure ionic liquids ([DAMI] [CF3CF2CF2CF2SO3] and [DAMI] [TfO]) and Ru-NPs (dispersed in same ionic liquid). Two phase model was used in this study. As per previous reports, we also found that the diameter of Ru-NPs larger than the ionic liquid thickness. The interface distribution function was applied on the experimental data to calculate the extended molecular length of both the ionic liquids (3.8 nm for [DAMI][CF3CF2CF2CF2SO3] and 1.7 nm for [DAMI][TfO]) [64–68]. A significant change in the L value was recorded due to the presence of Ru (0) nanoparticles for both the ionic liquids (Table 2; Fig. 2 in supplement information). Significantly higher increase in L value was observed with TfO^- anion mainly because of more ordered structural arrangement. The results obtained from correlation and interface distribution were found in good agreement with each other in Table 3. The cation mobility of ionic liquid was restricted mainly because of large $CF_3CF_2CF_2CF_2SO_3^-$ anion than TfO^- anion and such character hamper the formation of well-ordered Ru-NPs [51, 62, 63, 66, 67] (Fig. 3).

The SAXS analysis, concluded that the protective layer around the Ru (0) nanoparticle (mainly composed of semi-organized anionic species) present as supramolecular aggregates in following manner ([DAMI]x [X]x+1 x = 2 for X = CF3CF2CF2CF2SO3− anion and x = 3 for X = TfO− anion) with an extended molecular length of the 3.8 nm for [DAMI][CF3CF2CF2CF2SO3] and 1.7 nm for [DAMI][TfO] [67–70] .

The structural morphology of Ru-NPs was first studied by the TEM analysis before using them as catalyst (Fig. 2 in supplementary information). The structural influence of ionic liquids on the morphology of Ru-NPs, was found very effective (Table 2). It was clearly observed that the physiochemical properties like viscosity as well as ionic interaction between the cations and anions of the ionic liquid plays an important role on the structural features of

Ru-NPs such as stability, size, dispersion and agglomeration (Fig. 2 in supplementary information and Tables 2, 3) [38–43]. It is worth noted here that colloidal suspensions of the Ru-NPs in [DAMI] [CF3CF2CF2CF2SO3] ionic liquid medium were found stable up to for 10 days under argon atmosphere, while the suspensions of Ru-NPs in [DAMI] [TfO] ionic liquid. The Ru nanoparticles get separated from their corresponding ionic liquid just after 2–3 days. We can draw the conclusion (Table 1) that less coordinating ions (CF3CF2CF2CF2SO3−) prevents the separation of Ru-NPs from ionic liquid, better than TfO− anions. This unique effect of CF3CF2CF2CF2SO3− anions were dropped while lowering the carbon chain ([mammim] [CF3CF2CF2CF2SO3] ionic liquid) [38–47, 71–74].

3.3 CO_2 Hydrogenation Reaction in Ionic Liquid Mediated Ru (0) Nanocatalysts

The CO_2 Hydrogenation reaction was carried under H_2 atmosphere in the presence of Ru -NPs with both the ionic liquids separately at 50 °C. After 5 h, formic acid was isolated from the reaction mass followed by the nitrogen flow at 75–80 °C. The results obtained during reaction optimization with respect to TON/TOF value of formic acid were summarized in Table 4, entry 1–21. Acid–Base titration using phenolphthalein indicator and ^{1}H NMR analysis was used to calculate the quantity of formic acid formed after the hydrogenation reaction [72–74]. ^{1}HNMR analysis also confirmed no decomposition of formic acid as well as an ionic liquid during the experimental condition [72–74].

Initially, both ionic liquid immobilized Ru-NPs were tested under same reaction condition for CO_2 hydrogenation. Surprisingly, high TON/TOF value was obtained with [DAMI] [TfO] ionic liquid immobilized Ru NPs (Table 4, Entry 1 & 2) instead of [DAMI] [$CF_3CF_2CF_2CF_2SO$] mediated. This observation was found contradictory with respect to other published results, where smaller nanoparticles gave a high catalytic rate with respect to large nanoparticles [75]. The results obtained with [DAMI][TfO] immobilized Ru-NPs, confirmed that the surface of Ru-NPs is exposed or open for reactants as TfO− anions are less coordinated with respect to CF3CF2CF2CF2SO3− anions. To confirm this result, we designed a new set of experiments, where the [DAMI][TfO] mediated Ru-NPs were isolated and

Table 4 Hydrogenation of CO_2 to Formic acid using ionic liquid immobilized Ru NPs

Entry	Catalytic system	P (H_2) (P_{total}) (MPa)[a]	Temperature (°C)	Time (h)	TON[b]	TOF[c]
1	Ru NPs/[DAMI][$CF_3CF_2CF_2CF_2SO_3$]	25 (50)	30	5	1988	397.6
2	Ru NPs/[DAMI][TfO]	25 (50)	30	5	2014	402.8
3	Ru NPs/[DAMI][TfO]	25 (50)	50	5	22,680	4536.0
4	Ru NPs/[DAMI][TfO]	25 (50)	80	5	20,178	4035.6
5	Ru NPs/[DAMI][TfO]	25 (50)	100	5	19,872	3974.4
6	Ru NPs/[DAMI][TfO]	25 (50)	50	7	22,980	3282.9
7	Ru NPs/[DAMI][TfO]	25 (50)	50	2	19,862	9931.0
8	Ru NPs/[DAMI][TfO]	10 (20)	50	5	10,762	2152.4
9	Ru NPs/[DAMI][TfO]	30 (60)	50	5	22,710	4542.0
10	Ru NPs/ Ru NPs/[DAMI][TfO]$_+H_2O$ (1 mL)	25 (50)	50	5	23,221	4644.2
11	Ru NPs/ Ru NPs/[DAMI][TfO] + H_2O (2 mL)	25 (50)	50	5	24,525	4905.0
12	Ru NPs/ Ru NPs/[DAMI][TfO] + H_2O (3 mL)	25 (50)	50	5	23,861	4772.2
13	Ru NPs/ Ru NPs/[DAMI][TfO] (0.100 g) + H_2O (2 mL)	25 (50)	50	5	23,980	4796.0
14	Ru NPs/ Ru NPs/[DAMI][TfO] (0.500 g) + H_2O (2 mL)	25 (50)	50	5	24,545	4909.0
15	Ru NPs/ [DAMI][$CF_3CF_2CF_2CF_2SO_3$] + H_2O (2 mL)+	25 (50)	50	5	20,165	4033.0
16	$RuCl_3$ (0.07 g)[4]+ [DAMI][TfO] (0.100 g) + H_2O (2 mL)	25 (50)	50	5	10,210	2042.0
17	Ru NPs/ [mammim][$CF_3CF_2CF_2CF_2SO_3$] + H_2O (2 mL)	25 (50)	50	5	20,138	4027.6
18	Ru NPs/ [mammim][TfO]$_+$ H_2O (2 mL)	25 (50)	50	5	19,028	3805.6
19	$RuCl_3$ (0.07 g)[d] + [DAMI][TfO] (0.100 g) + H_2O (2 mL)	25 (50)	50	5	780	156.0
20	Ru NPs + H_2O (2 mL)	25 (50)	50	5	23	4.6
21	Ru NPs	25 (50)	50	5	–	–

[a]The total pressure of the system is indicated in parentheses

[b]Turn over number = n (formic acid) n $(Ru)^{-1}$ in one reaction cycle

[c]Turnover frequency = n (formic acid) n $(Ru)^{-1}$ h^{-1}

[d]$RuCl_3 \cdot xH_2O$ (50% Ru metal)

Table 5 Reaction optimization for in situ generated Ru NPs for CO_2 hydrogenation

Entry	Temperature (°C)	$P(H_2)$ (P_{total}) (MPa)	Time (h)	TON[a]	TOF[b]
1	50	50	5	26,525	
2	80	50	5	20,178	
3	100	60	5	26,551	
4	50	50	2.5	21,514	
5	50	50	8	26,575	

[a]Turn over number = n (formic acid) n $(Ru)^{-1}$ in one reaction cycle

[b]Turnover frequency = *n* (formic acid) n $(Ru)^{-1}h^{-1}$

re-dispersed in [DAMI][CF3CF2CF2CF2SO] ionic liquid. The same exercise was performed for [DAMI] [CF3CF2CF2CF2SO] mediated Ru-NPs and the recovered Ru-NPs were re-dispersed in [DAMI] [TfO] ionic liquid. This modified ruthenium dispersion was applied to CO2 hydrogenation reaction. Formic acid with low TON values obtained from highly coordinated CF3CF2CF2CF2SO− anions with respect to less coordinated TfO− anions. It is worth noted that the miscibility of reactants is almost similar to both the ionic liquids. Such observations also confirmed that the Ru-NPs are surrounded by the anions of ionic liquid [69, 75].

Other important reaction parameters and technical variables were investigated with [DAMI][TfO] immobilized Ru-NPs (Table 4, Entry 3–15). While optimizing the reaction temperature for hydrogenation reaction, we obtained good TON/TOF value at lower temperature (50 °C), when the total H2/CO2 gas pressure was 50 MPa (Table 4, Entry 3–5). Effect of water was also studied on the reaction kinetics of CO2 hydrogenation reaction and with 2 ml of water; we obtained the formic acid with a high TON/TOF value (Table 4, entry 12) mainly because CO2 may react with water as well as amine group of ionic liquid and offers bicarbonates which may act as a perfect substrate for the hydrogenation reaction. RuCl3·3H2O was also evaluated in [DAMI][TfO] for hydrogenation reaction, but formic acid was obtained with a low TON/TOF value with respect to [DAMI][TfO] immobilized Ru NPs (Table 4, Entry 16) [72–74].

After getting friendly results with [DAMI][TfO] ionic liquid immobilized Ru-NPs with water, we shifted our study to catalytic hydrogenation of CO_2 to formic acid followed by in situ generated Ru-NPs in ionic liquid. To achieve this task, we started the reaction with synthesizing Ru-NPs in [DAMI] [TfO] ionic liquid from $[RuCl_2(C_6H_6)]_2$. After synthesizing the ionic liquid mediated Ru-NPs, optimized quantity of water and then CO_2/H_2 gases were added

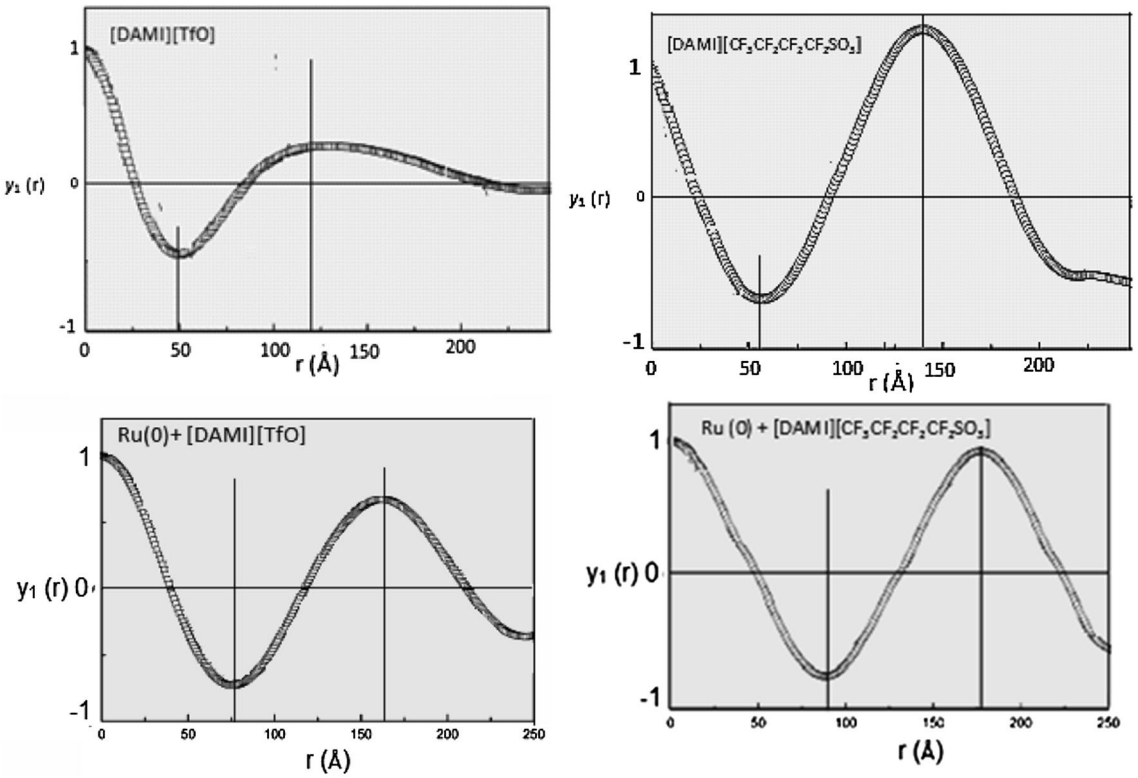

Fig. 3 Plots of correlation function of ionic liquid and ionic liquid mediated Ru(0) nanoparticles

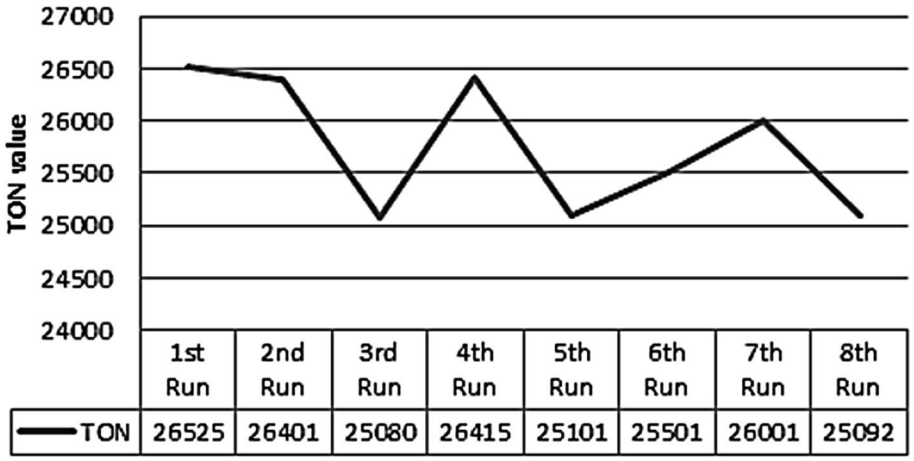

Fig. 4 Catalyst recycling test for Ru(0)+[DAMI][TfO] catalytic systems

in the reaction vessel (without opening the lid of vessel). After heating the reaction mass at the 50 °C for 5 h, we successfully obtained the formic acid with a good TON / TOF value (Table 5, Entry 1). Reaction parameters such as time, temperature and the quantity of CO_2/H_2 gases were again optimized for in situ generated Ru NPs in [DAMI] [TfO] (Table 5, Entry 1–6). Higher TON/TOF value of formic acid was obtained with respect to standing Ru nanoparticles for the normal above mentioned reaction mainly because of Ru metal loss during the catalyst isolation step of catalyst preparation.

Formic acid was isolated from reaction mass with the aid of N_2 gas and the [DAMI] [TfO] ionic liquid immobilized Ru NPs went for a recycling test (after washing with diethyl ether). [DAMI] [TfO] ionic liquid immobilized Ru NPs were recycled up to 7 times with slight loss of their catalytic activity mainly because of agglomeration of Ru NPs which was also confirmed by TEM analysis of Ru NPs (Fig. 4). Significant increase, in the particle size of Ru NPs from 8.1 (±0.5) nm to 15.5 (±0.5) nm *(due to the agglomeration of Ru NPs)* may cause a drop in the catalytic activity of Ru NPs during recyclability test.

4 Conclusion

We developed nine different types of ruthenium nanoparticles using five types of ruthenium precursors and four types of ionic liquids. All the materials were properly analyzed by sophisticated analytical techniques. XRD analysis of isolated ruthenium nanoparticles showed that well-coordinated and small size nanoparticles were obtained with [DAMI] [$CF_3CF_2CF_2CF_2SO_3$] ionic liquids over [DAMI] [TfO] ionic liquid. The XPS analysis also confirmed the presence of ruthenium nanoparticles as Ru(0) species in the system. SAXS analysis along with XRD and XPS data confirmed the surrounding of ionic liquid protective layer around ruthenium nanoparticles. Additionally, high catalytic activity of the [DAMI][TfO] mediated ruthenium nanoparticles was observed in CO_2 hydrogenation reaction with respect to other catalytic systems. Increase in catalytic activity was observed mainly due to the presence of less coordinated Ru (0) species in [DAMI][TfO]ionic liquid.

Apart from the above observations, we successfully synthesized *insitu* ruthenium nanoparticles in ionic liquid medium and successfully applied for CO_2 hydrogenation reaction. The insitu catalytic system was found highly active in terms of high TON/TOF value over above mentioned systems. Subsequently, the catalytic system was recycled up to eight catalytic runs.

Acknowledgements This work is financially supported by DST Fast Track (SB/FT/CS-124/2012), India.

References

1. Friedlingstein P (2010) Nat Geosci 3:811
2. Shindell DT (2009) Science 326:716
3. Archer D, Brovkin V (2008) Clim Change 90:283
4. Zhang Z, Hu S, Song J, Li W, Yang G, Han B (2009) Chem Sus Chem 2:234
5. Budzianowski WM (2012) Energy 41:280
6. Varre SBK, Siriwardane HJ, Gondle RK, Bromhal GS, Chandrasekar V, Sams N (2015) Int. J Greenhouse Gas Control 42:138
7. Liu Q, Maroto-Valer MM (2011) Greenhouse Gases 1:211
8. Najafabadi AT (2013) Int J Energy Res 37:485
9. Li Y, Chan SH, Sun Q (2015) Nanoscale 7:8663
10. Gomes CDN, Jacquet O, Villiers C, Thuéry P, Ephritikhine M, Cantat T (2011) Angew Chem Int Ed 51:187
11. Sivashunmugam S, Kannan S (2012) Indian J Chem 51A:1252
12. You H, Yang S, Ding B, Yang H (2013) Chem Soc Rev 42:2880
13. Gaffet E (2011) C R Phys 12:648
14. Kim BH, Hackett MJ, Park J, Hyeon T (2014) Chem Mater 26:59
15. Duan H, Wang D, Li Y (2015) Chem Soc Rev 44:5778
16. Andrievski RA (2014) J Mater Sci 49:1449

17. Prieto G, Zečević J, Friedrich H, de Jong KP, de Jongh PE (2013) Nat Mater 12:34
18. Campbell CT, Parker SC, Starr DE (2002) Science 298:811
19. Farmer JA, Campbell CT (2010) Science 329:933
20. Zhang Y, Erkey C (2006) J Supercrit Fluids 38:252
21. White RJ, Luque R, Budarin VL, Clark JH, Macquarrie DJ (2009) Chem Soc Rev 38:481
22. Sarkar S, Guibal E, Quignard F, Gupta AKS (2012) J Nanopart Res 14:715
23. He Z, Alexandridis P (2015) Phys Chem Chem Phys 17:18238
24. Campelo JM, Luna D, Luque R, Marinas JM, Romero AA (2009) Chem Sus Chem 2:18
25. Welton T (1999) Chem Rev 99:2071
26. Dupont J, Scholten JD (2010) Chem Soc Rev 39:1780
27. Wilkes JS, Wasserscheid P, Welton T (2007) Introduction. In: Wasserscheid P, Welton T (eds). Wiley-VCH Verlag GmbH & Co. KGaA, Hoboken ch. 1
28. Holbrey JD, Rogers RD, Mantz RA, Trulove PC, Cocalia VA, Visser AE, Anderson JL, Anthony JL, Brennecke JF, Maginn EJ, Welton T, Mantz RA (2007) Physicochemical properties. In: Wasserscheid P, Welton T (eds). Wiley-VCH Verlag GmbH & Co. KGaA, Hoboken ch. 3
29. Earle MJ, Esperança JMSS, Gilea MA, Lopes JNC, Rebelo LPN, Magee JW, Seddon KR, Widegren JA (2006) Nature 439:831
30. Liviano SR, Nuñez NO, Fernández SR, de la Fuente JM, Ocaña M (2013) Langmuir 29:3411
31. Hatakeyama Y, Judai K, Onishi K, Takahashi S, Kimura S, Nishikawa K (2016) Phys Chem Chem Phys 18:2339
32. Lei Z, Dai C, Chen B (2014) Chem Rev 114:1289
33. Upadhyay PR, Srivastava V (2016) RSC Adv 6: 42297
34. Cadena C, Anthony JL, Shah JK, Morrow TI, Brennecke JF, Maginn EJ (2004) J Am Chem Soc 126:5300
35. Bates ED, Mayton RD, Ntai IH (2002) J Am Chem Soc 124:926
36. Soriano AN, Doma BT Jr, Li M-H (2008) J Chem Eng Data 53:2550
37. Scovazzo P, Kieft J, Finan DA, Koval C, DuBois D (2004) J Membr Sci 238:57
38. Migowski P, Dupont J (2007) Chem A Eur J 13:32
39. Wender H, de Oliveira LF, Migowski P, Feil AF, Lissner E, Prechtl MHG, Teixeira SR, Dupont J (2010) J Phys Chem C 114:11764
40. Dupont J (2004) J Braz Chem Soc 15:341
41. Gallon BJ, Kojima RW, Kaner RB, Diaconescu PL (2006) Angew Chem Int Ed 45:7251.
42. Dupont J, Suarez PAZ (2006) Phys Chem Chem Phys 8:2441
43. Canongia Lopes JNA, Padua AAH (2006) J Phys Chem B 110:3330
44. Alencar M, Meneghetti MR, Dupont J, Hickmann JM (2008) J Phys 20:155102
45. Migowski P, Machado G, Texeira SR, Alves MCM, Morais J, Traverse A, Dupont J (2007) Phys Chem Chem Phys 9:4814
46. Gutel T, Santini CC, Philippot K, Padua A, Pelzer K, Chaudret B, Chauvin Y, Basset JM (2009) J Mater Chem 19:3624
47. Redel E, Thomann R, Janiak C (2008) Inorg Chem 47:14
48. Rossi LM, Dupont J, Machado G, Fichtner PFP, Radtke C, Baumvol IJR, Teixeira SR (2004) J Braz Chem Soc 15:904
49. Yinghuai Z, Widjaja E, Sia SLP, Zhan W, Carpenter K, Maguire JA, Hosmane NS, Hawthorne MF (2007) J Am Chem Soc 129:6507
50. Silveira ET, Umpierre AP, Rossi LM, Machado G, Morais J, Soares GV, Baumvol IJR, Teixeira SR, Fichtner PFP, Dupont J (2004) Chem A Eur J 10:3734
51. Samon JM, Schultz JM, Hsiao BS (2000) Polymer 41:2169
52. Yang P-W, Liu Y-T, Hsu S-P, Wang K-W, Jeng U-S, Lina T-L, Chen T-Y (2015) Cryst Eng Comm 17:8623
53. Ran S, Zong X, Fang D, Hsiao BS, Chu B, Phillips RA (2001) Macromolecules 34:2569
54. Nam JY, Kadomatsu S, Saito H, Inoue T (2002) Polymer 43:2101
55. Matsui S, Kureha T, Nagase Y, Okeyoshi K, Yoshida R, Sato T, Suzuki D (2015) Langmuir 31:7228
56. Bhattacharyya AR, Ghosh AK, Mishra A (2001) Polymer 42:9143
57. Sankaran V, Cohen RE, Cummins CC, Schrock RR (1991) Macromolecules 24:6664
58. Nasedkin A, Marcellini M, Religa TL, Freund SM, Menzel A, Fersht AR, Jemth P, van der Spoel D, Davidsson J (2015) PLoS ONE 10:1
59. hee H, Wulff M, Kim J (2010) Int Rev Phys Chem 29:453
60. Kaper H, Endres F, Djerdj I, Antonietti M, Smarsly BM, Maier J, Hu Y-S (2007) Small 3:1753
61. Supaphol P, Lin JS (2001) Polymer 42:9617
62. Cola ED, Grillo I, Ristori S (2015) Pharmaceutics 8:1
63. Ciebien JF, Cohen RE, Duran A (1998) Supramol Sci 5:31.
64. Ruland W (1977) Colloid Polym Sci 255:417
65. Hsiao BS, Wang ZG, Yeh F, Gao Y, Sheth KC (1999) Polymer 40:3515
66. Verma R, Marand H, Hsiao B (1996) Macromolecules 29:7767
67. Cruz CS, Stribeck N, Zachmann HG, Calleja FJB (1991) Macromolecules 24:5980
68. Korgel BA, Fitzmaurice D (1999) Phys Rev B 59:14191
69. Scheeren CW, Machado G, Teixeira SR, Morais J, Domingos JB, Dupont J (2006) J Phys Chem B 110:13011
70. Liu J, Han B, Zhang J, Li G, Zhang X, Wang J, Dong BZ (2002) Chem Eur J 8:1356
71. Hornstein BJ, Finke RG (2004) Chem Mater 16:3972–3972 (**2004**)
72. Srivastava V (2014) Catal Lett 144:1745
73. Srivastava V (2014) Catal Lett 144:2221
74. Upadhyay P, Srivastava V (2016) Catal Lett 146:12
75. Cassol CC, Ebeling G, Ferrera B, Dupont J (2006) Adv Synth Catal 348:243